SURFACE WAVE DISPERSION MEASUREMENTS AND TOMOGRAPHY FROM AMBIENT SEISMIC NOISE CORRELATION IN CHINA

Xiaodong Song[1], Zhen Xu[1], Xinlei Sun[1], Sihua Zheng[2], Yingjie Yang[3], and Michael H. Ritzwoller[3]

The University of Illinois at Urbana-Champaign[1], the Institute of Earthquake Science, China Earthquake Administration[2], and the University of Colorado at Boulder[3]

Sponsored by the Air Force Research Laboratory

Contract No. FA8718-07-C-0006
Proposal No. BAA07-24

ABSTRACT

We perform ambient noise tomography of China using the data from the China National Seismic Network and surrounding global and PASSCAL stations. The results so far are summarized below. (1) Dispersion measurements and tomography. For most of the station pairs, we retrieve good Rayleigh waveforms from ambient noise correlations using 18-months of continuous data at all distance ranges across the entire region (over 5000 km) and for periods from 70 s down to about 8 s. We obtain Rayleigh wave group and phase velocity dispersion measurements using a frequency-time analysis method and invert for Rayleigh dispersion maps for periods from 8 to 60 s. The dispersion maps correlate nicely with surface geology. (2) Error estimates using bootstrap analysis. A major feature of the ambient noise method is that the whole process is completely repeatable with different time segments, which make it possible to evaluate the uncertainties. We adopt a bootstrap method to quantify the errors in the Rayleigh wave group velocity dispersion measurements and the tomographic maps. Most of the pairs show similar dispersion curves between different runs and small standard deviations, indicating good data quality and convergence of the Green function. Group velocity at long period end generally has a larger error, which is consistent with the notion that the long period needs longer time to converge. The best retrieved periods are from 10 to 30 s with the optimal period of around 15 to 20 s.

Pairs with large errors do not depend on the orientations of the paths or the locations of the stations. Rather, they are associated with a few stations with large average standard errors. The likely causes are missing data and poor instrumentation (or site conditions). Where ray coverage is good, there is only subtle difference in tomography maps between different runs, suggesting that our solution is very stable. (3) 3D structure. We invert the Rayleigh group and phase dispersion maps for 3D shear-wave velocity structure. The 3D model shows some remarkable features, including slow sedimentary layers of all the major basins in China at the shallow depth, Moho depth variation, fast (strong) mid-lower crust and mantle lithosphere in major basins surrounding the Tibetan Plateau (TP) (Tarim, Ordos, and Sichuan). These strong blocks thus seem to play an important role in confining the deformation of the TP to be a triangular shape. The Moho change from plateau to the marginal basins (Tarim and Sichuan) is rapid, corresponding to the rapid change of the surface topography. In northwest TP, slow anomalies extend from shallow crust to mantle lithosphere (at least 100 km). Widespread, prominent low-velocity zone is observed in mid-crust in much of the TP, but not in the margin areas, consistent with the crustal channel flow model.

OBJECTIVES

The overall objective of this project is to obtain surface wave dispersion measurements from ambient seismic noise correlations of the Chinese backbone stations (CNSN) and use these measurements to produce surface wave dispersion maps of China. More specifically, the objectives are: (1) to obtain dispersion measurements between CNSN stations; (2) to obtain dispersion measurements between CNSN and FDSN, regional networks, and temporary stations; (3) to obtain dispersion maps from these dispersion measurements.

RESEARCH ACCOMPLISHED

We reported the basic metholodgy, data sets, and initial results in the last year's review (Song et al., 2008), part of which has also been published in Zheng et al. (2008). Below is an update to that report. In this report, we nearly double the amount of the data and the number of stations used, and as a result, we provide new dispersion measurements, dispersion maps, and 3D velocity model. We have also conducted resolution tests of our 3D inversion.

Method and Data

Theoretical and laboratory studies have shown that the Green functions of a structure can be obtained from the cross-correlation of diffuse wavefields (e.g., Lobkis and Weaver, 2001; Campillo, 2006). The basic idea is that linear waves preserve, regardless of scattering, a residual coherence that can be stacked and amplified to extract coherent information between receivers. The idea has found rapid applications in seismology. In particular, surface waves have been found to be most easily retrievable from the cross-correlations of seismic coda (Campillo and Paul, 2003) or ambient noise (Shapiro et al., 2005; Sabra et al., 2005) between two stations. Both Rayleigh waves and Love waves can be retrieved. The new type of data has rapidly been used for tomographic mapping at regional or local scales and on continental scales. Most studies have focused on Rayleigh wave group velocity tomography from ambient noise. However, the method is applicable to Love waves and phase velocity measurements.

Ambient noise tomography (ANT) overcomes several important limitations of conventional methods based on earthquakes; i.e., uneven distribution of earthquake sources, uncertainty in earthquake location, and attenuation of short-period surface waves. Thus, the method is particularly useful for surface-wave path calibration and for tomographic mapping in aseismic regions especially at short periods (below 30 s). In addition, the method can be applied any time without the need to wait for earthquakes and is completely repeatable, allowing the quantification of errors.

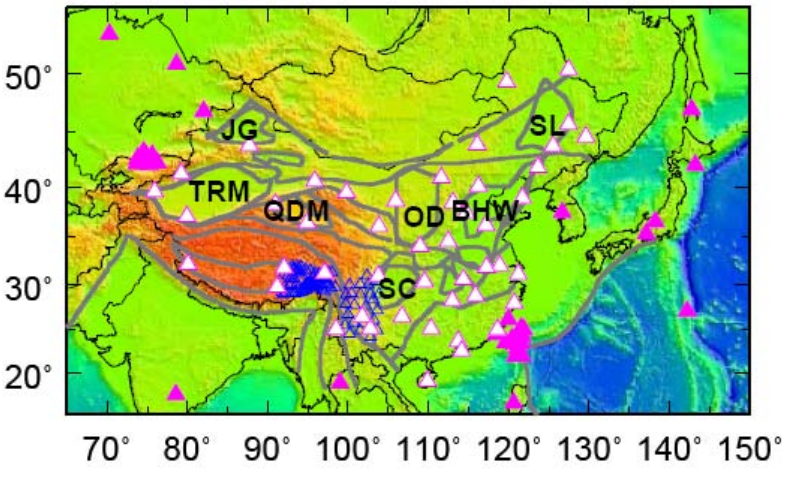

Figure 1. Distribution of seismic stations used in this study, including China National Seismic Network (CNSN) stations (solid white triangles), global and regional stations in the surrounding regions (solid pink triangles), and PASSCAL stations (open blue triangle). We have also used some 175 temporary stations in western Tibet from HiClimb not included in this map. Plotted also are major tectonic boundaries and major basins. The basins (labeled) include: Tarim (TRM), Junggar (JG), Qaidam (QD), Sichuan (SC), Ordos (OD), Bohai Wan (BHW), and Songliao (SL) Basins.

Our main stations are from the China National Seismic Network (CNSN) (Figure 1). The CNSN is the national backbone network, established around 2000, with a relatively uniform distribution across the continental China. To increase data coverage, we also include permanent and temporary stations in the region. We use 12 or more months of continuous data from 47 CNSN stations and 39 stations in surrounding regions and some 270 PASSCAL stations in the TP. All stations are broadband. The bandwidths of the CNSN stations are from 20 Hz to at least 120 s. We use the data processing and imaging techniques described in great detail by Bensen et al. (2007). Below is a brief outline of our data procedure. First, we obtain the empirical Green function (EGF) from ambient noise cross-correlation. Continuous data are pre-processed before correlation and stacking, which includes clock synchronization, removal of instrument response, time-domain filtering, temporal normalization and spectral whitening. The purpose is to reduce the influence of earthquake signals and instrument irregularities and to enhance the strength and bandwidth of the ambient noise correlations. Second, if the signal-to-noise ratio (SNR) is sufficiently large, Rayleigh wave group speeds are measured using a frequency-time analysis (Ritzwoller and Levshin, 1998). Finally, the inter-station dispersion measurements are used to invert for the Rayleigh wave group velocity maps, in exactly the same way as earthquake-based measurements.

Dispersion Measurements and Tomography

For most of the station pairs, we are able to retrieve good Rayleigh wave signals from the ambient noise correlations (Zheng et al., 2008). Figure 2 shows typical examples of EGFs and group velocity measurements of Rayleigh waves retrieved from ambient noise correlations. Our cross-correlations show clear arrivals at different settings (near the coast or well into the continental interior) and at both relatively low frequencies (20-50 s) and high frequencies (5-20 s). The EGFs can be retrieved over the entire region (at distances of over 5000 km) (Figure 2a).

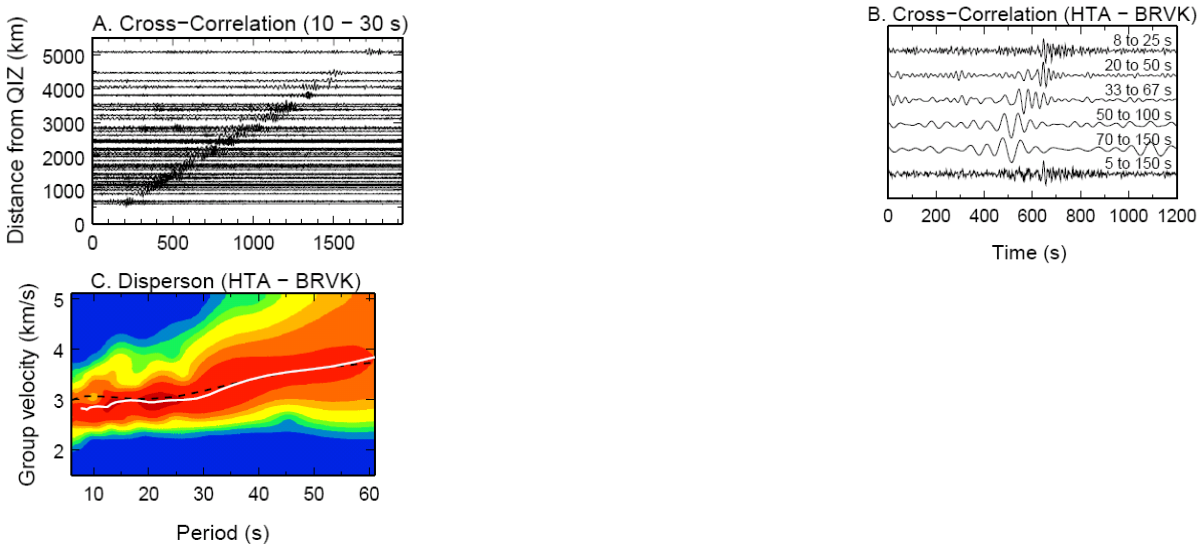

Figure 2. **Example of Rayleigh wave EGFs and dispersion measurements obtained from ambient noise correlations. (a) Symmetric component of the correlations between station QIZ (in Hainan Province, China) and other stations. The traces are band-pass filtered at relatively short periods (10-30 s). (b) EGFs filtered in different frequency bands. Long-period surface waves are clearly faster than short-period ones. The path is between HTA (bordering Tarim in the south) and BRVK (Borovoye, Kazakhstan). (c) Frequency-time analysis (Ritzwoller and Levshin, 1998) used to retrieve Rayleigh wave group velocity dispersion curve (white) for the HTA-BRVK path. The black dashed curve is the prediction from the 3D global shear velocity model of Shapiro and Ritzwoller (2002), which is used for phase-matched filtering in the data analysis and for comparison with measurements**.

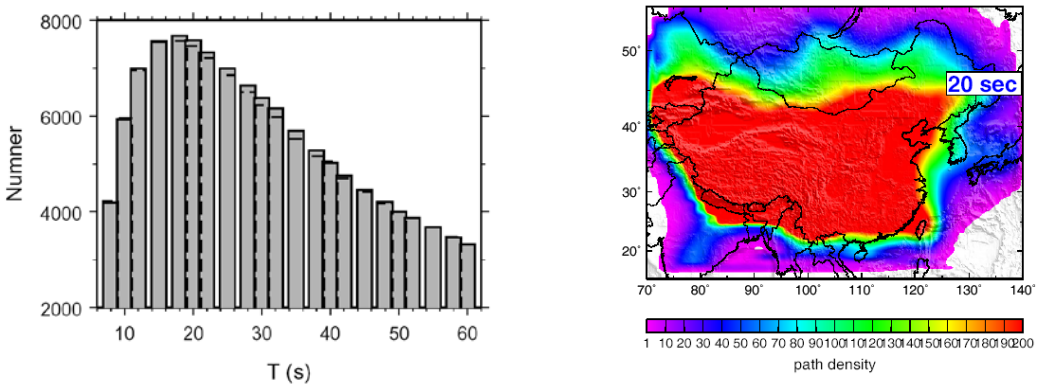

Figure 3. **Distribution of Rayleigh group (solid) and phase (dashed) dispersion measurements for different periods (left) and ray density map for Rayleigh group dispersion measurements at the period of 20 s (right). The ray density is the number of rays inside 1 degree by 1 degree cell. The rays are station pairs for which dispersion measurements have been obtained. The ray coverage is best for periods 10 to 30 s. Coverages for shorter or longer periods deteriorate, but the spatial coverage patterns remain similar.**

We measured group velocity dispersion curves (Figure 2c) for station pairs with Rayleigh wave SNR>10. The SNR is defined as the ratio of the peak amplitude of the Rayleigh wave to the root-mean-square value of the background. The measurement is very stable. Clear dispersion can be commonly observed directly from the EGFs (**Figure 2b**). We found that the group velocity measurements can extend to periods of 10 s or shorter even for station pairs that are separated over thousands of kilometers. The group velocities of the HTA-BRVK path (**Figure 2b,c**), which samples the Tarim Basin, agree with a global 3D earthquake-based model (Shapiro and Ritzwoller, 2002) at longer periods but differ significantly at short periods (below 30 s). The slow group velocities at short periods are caused by the thick sediments of the Tarim Basin (see discussion below).

We have obtained dispersion measurements with SNR>10 for periods 8 s to 70 s (Figure 3, left). The best observed frequency band is 10 to 30 s with a retrieval rate of 50 to 80% of all the possible pairs. The ray paths provide good coverage of almost the entire Chinese continent except at the margins (Figure 3, right).

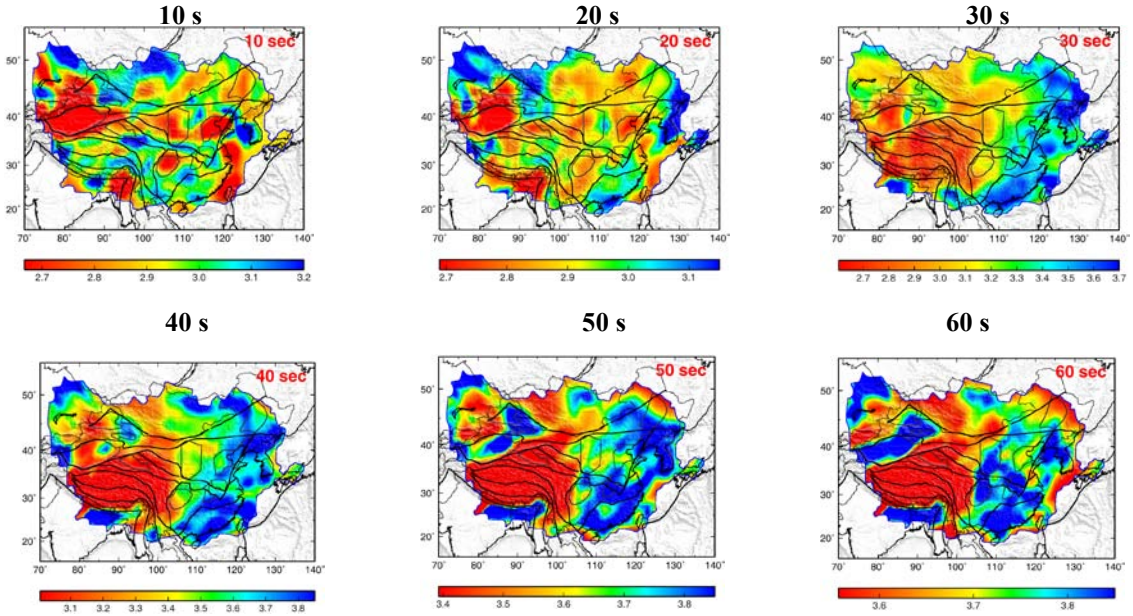

Figure 4. **Rayleigh wave group velocities obtained in this study. Shown are the maps at periods 10 to 60 s, respectively. Plotted in the background are major block boundaries and basin outlines (Figure 1).**

The ray coverage of our dispersion measurements is sufficient for us to invert for Rayleigh wave group velocity maps at periods from 8 s to 60 s (Figure 4). The results show remarkable features that correlate with large-scale geological structures of China (discussed in more details in Zheng et al., 2008). Major basins are well delineated with low velocities at short periods (8 to 20 s), including Bohai-Wan Basin (North China Basin), Sichuan Basin, Qaidam Basin, and Tarim Basin. The stable Yangtz Craton also shows up well with high velocities. At longer periods (25-50 s), the group velocity maps display striking bimodal distribution with high velocity in the east and low velocity in the west, which corresponds very well with the thinner crust in the east and much thicker crust in the west (e.g. Liang et al., 2004) as in global reference model CRUST 2.0 (http://mahi.ucsd.edu/Gabi/rem.html). The NNE-SSW trending boundary between fast and slow velocities (around longitude 108^{o}E) coincides with the sharp topographic change and with the well-known Gravity Lineation.

3D shear-wave Structure

We use the Rayleigh wave group and phase velocity maps (8-60 s) obtained from the ANT to invert for 3D S structure. The inversion is done using programs by Bob Herrmann of St. Louis U. Resolution tests suggest that a 4x4 degree pattern can be resolved in most region of China (Figure 5). The inversion results show some remarkable features for continental China and in particular the Tibetan Plateau (TP) (Figure 6), including slow sedimentary layers of all the major basins at the shallow depth, striking east-west contrasts in Moho depth variation and lithosphere thickness, fast (strong) mid-lower crust and mantle lithosphere in major basins surrounding the TP (Tarim, Ordos, and Sichuan) (in contrast, Qaidam Basin does not have such a "deep root"). These strong blocks thus seem to play an important role in confining the deformation of the TP to be a triangular shape. The Moho change from plateau to the marginal basins (Tarim and Sichuan) is rapid, corresponding to the rapid change of the surface topography. . In northwest TP, slow anomalies extend from shallow crust to mantle lithosphere (at least 100 km).

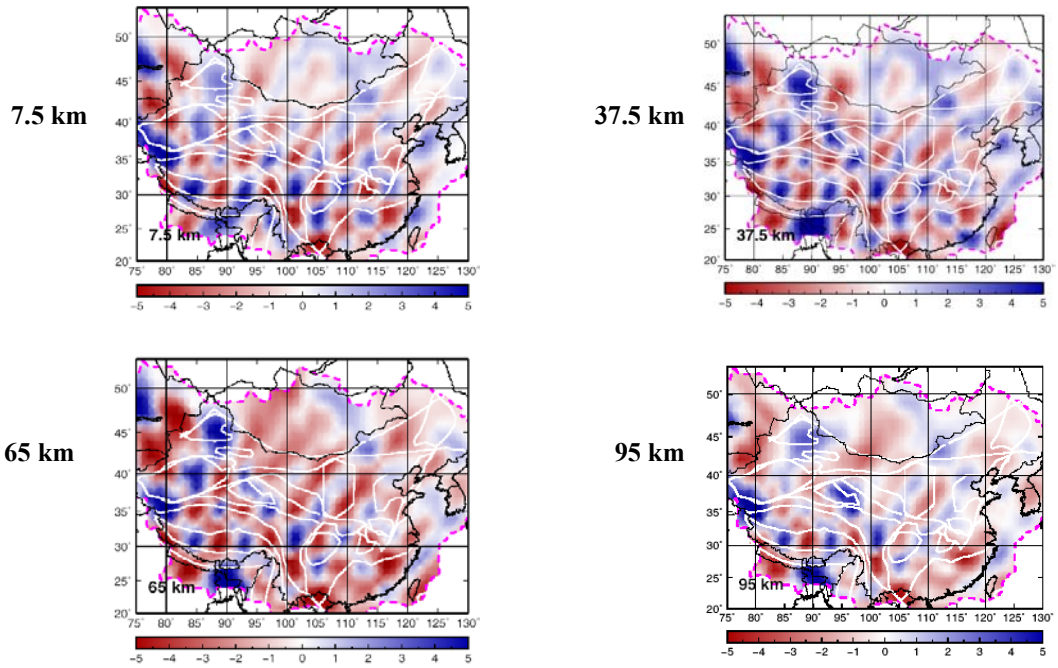

Figure 5. Results of a checker-board test. The input is alternating pattern of 4x4 degrees with S velocity perturbations of 5%.

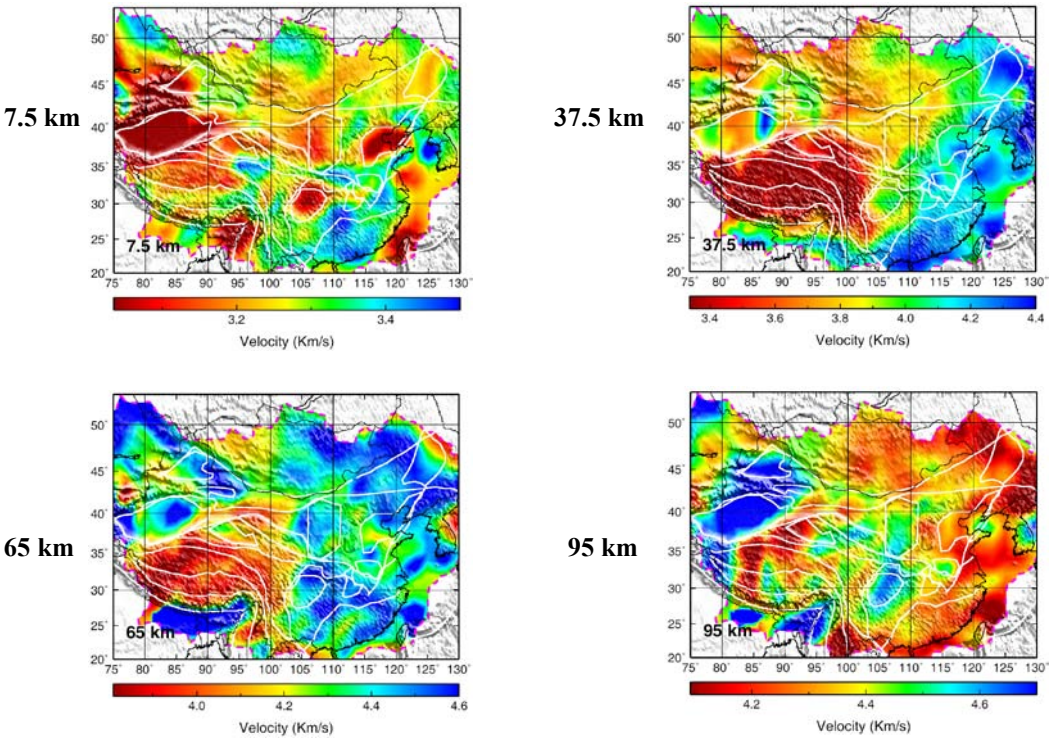

Figure 6. **Inversion results of S velocity at 7.5, 37.5, 65, and 95 km.**

Extremely slow *S* velocities mark the mid-crust in much of the central, eastern, and southeastern TP. These slow velocities are widespread and often (but not always) connected in a laminar form. They seem to reach to the surface at certain localities in western, southern, northern, and southeastern margins. The mid/lower crust low velocity zone provides support for the channel flow model that has been proposed for the outward growth and uplift of the TP (e.g. Clark and Royden, 2000) and for the extrusion of crustal materials to the surface (Beaumont et al., 2001).

We are exploring the S velocity model we have derived on its characters and tectonic implications. Because of the apparent correlation of the S velocities and crustal thickness, one useful exercise is to derive a crustal thickness model based on the Vs model. If we obtain the Vs that corresponds to the depth of the Moho as defined by the reference model CRUST 2.0, we find that the average of the S velocities is nearly constant (Figure 7). We thus use the linear trend as a calibration of using the *S* velocity to find the true Moho (The linear trend has nearly the same Vs value with only a small positive slope). Thus to find the true Moho for any given point, we follow the steps: (1) Find the reference Moho depth from CRUST 2.0, (2) find the reference Vs from the linear trend, and (3) find the depth that corresponds to the reference Vs (and close to the CRUST 2.0 depth). The procedure ensures that the newly derived Moho map (Figure 8, left) is similar to the CRUST 2.0 (Figure 8, right) overall, but the new map shows detailed variations that correspond to variation in *S* velocities.

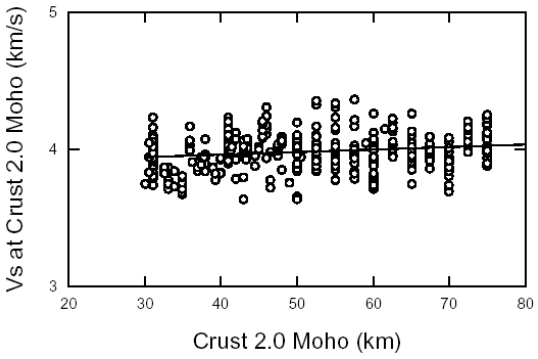

Figure 7. *S* velocities at the depth of CRUST 2.0 Moho that are retrieved from our *S* model.

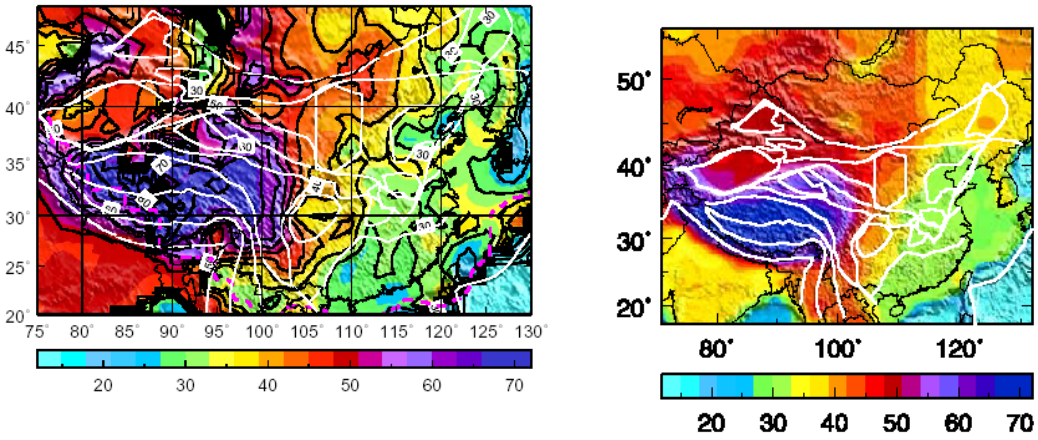

Figure 8. Crustal thickness map derived from the *S* velocity model (left), in comparison to reference CRUST 2.0 model (right). Note the map scales are different.

Validation and Error Analyses of Dispersion Measurements and Tomography

We have examined the errors of our dispersion measurements and tomography in a variety of ways (see a summary by Zheng et al., 2008). The methods include the following. (1) Validation with surface observables. Comparison of the tomographic maps with the geological features discussed above provides an important initial validation of the ambient noise tomography (ANT) methodology; i.e., the method provides models of group wave speeds that are consistent with well-known geological features and other geophysical observations. (2) Direct validation with surface wave generated by an earthquake along the same path (e.g., Shapiro et al., 2005; Bensen et al., 2007). (3) Comparing EGFs obtained from ambient noise and that from seismic coda (Yao et al., 2006). (4) Temporal stability: Comparing the EGFs from the data observed at different time periods (e.g., different months) (Shapiro et al., 2005; Yao et al., 2006; Bensen et al., 2007). Furthermore, because the principal ambient noise sources are believed to come from the oceans, which are seasonal, the consistency of the correlations from different seasons gives a measure of the stability and error of the EGFs. (5) Spatial consistency: Comparing station-pairs along similar paths (Bensen et al., 2007). The EGFs between a far-away station to two or more stations that are close to one another should be similar as the paths sample similar structure. We have examined temporal and spatial consistency of our dispersion measurements and found that they are very consistent whenever the SNRs of the EGFs are high (see examples in Zheng et al., 2008). (6) Model-based validation: comparing predictions with earthquake-based measurements (Figure 9). (7) Bootstrap analyses (Xu et al., 2008) (see below).

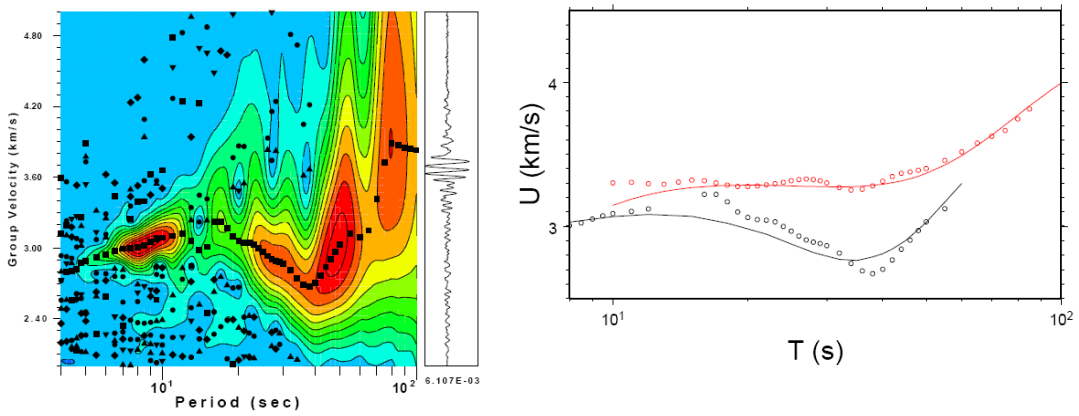

Figure 9. (Left) Retrieval of Rayleigh wave group velocity of a 2008 Wenchuan aftershock at Lhasa station. (Right) Comparison of observed (dots) and predicted group velocities of Rayleigh (black) and Love (red) waves along the path. Lines are predictions for the ambient noise tomographic model. The retrieval of the surface wave EGF relies on the stacking of cross correlation of continuous data for long enough time series. The total length of data required for the Green function to converge is empirical and highly frequency

dependent: generally the longer the period the longer the time is needed. Furthermore, the ambient noise source and station site conditions (including instrumentation stability) are uncertain. We have recently proposed a bootstrap method to quantify the errors in Rayleigh group velocity dispersion measurements and group velocity tomographic maps, based on the complete repeatability of the ambient noise correlation and tomography process (Xu et al., 2008).

Our bootstrap analysis follows the following steps. 1) We obtain the EGF using one month of data for each of the 18 months. 2) We select 18 random months among the months that we have data. The selection process is a random sampling with replacement as in any boostrap methods. We then obtain the statck EGF using the EGFs of these months for each and every station pair. Using these stacked GFs, we measure dispersion curves for all station pairs and construct tomographic maps as usual. 3) We repeat the step 2 for 50 times. 4) We obtain the mean and the standard deviation of the dispersion curve for each station pair from the 50 dispersion curves obtained in step 3. We regard the mean and the standard deviation as the group velocity estimate and the associated error. 5) Similarly, we obtain the standard errors of our tomographic models using the models obtained from the 50 iterations described in steps 2 and 3.

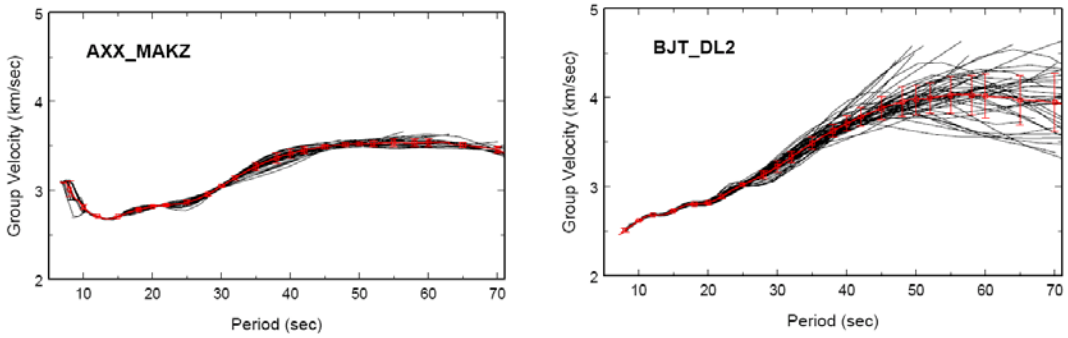

Figure 10. Examples of error estimates of dispersion curves from bootstrap with a good pair (left) and a bad pair (right). Black curves are dispersion measurements for all the 50 runs. Red curves are the mean values. Error bars at different periods indicate the standard deviations. For the good pair (AXX-MAKZ), dispersion curves for different runs are very close to each other. The standard deviations are small throughout the whole periods. For the bad pair (BJT-DL2), dispersion curves spread out at long periods. The large standard deviations at long periods indicate large errors in the measurements.

Figure 10 shows two examples of error estimates of the dispersion curves using the boostrap method. Most pairs show similar dispersion curves between different runs and small standard deviation (generally less than 0.1 km/s), indicating good data quality and convergence of the Green function. Group velocity at a long period generally has a larger error, which is consistent with the notion that the long period needs longer time to converge. There is only subtle difference in tomography maps between different runs, suggesting that our solution is very stable. Standard deviation in the region with good ray coverage is small (generally less than 0.1 km/s), indicating a stable and reliable solution in well-sampled regions. The Rayleigh waves are best retrieved from 10 to 30 s with the best periods around 15 to 20 s. A pitfall of the model error estimates is that the standard deviations in the regions with poor ray coverage (at the margins) are also small, due to regularization in the tomographic inversion process. Our tomographic inversion includes regularization using a prior model. Thus the inversions for the poorly sampled regions from different runs all converge to the prior model, giving an artifact of small errors.

We found that the pairs with large variations do not have a preferred orientation or a particular geographical location. Rather, these pairs are generally associated with a few stations with large standard deviations. We derive average standard deviation of the surface wave velocity for each station at each period by averaging over all the pairs associated with that station. The exercises provide a way to identify and sort out good and poor stations efficiently.

CONCLUSIONS AND RECOMMENDATIONS

We have obtained Rayleigh dispersion curves for some 30,000 station pairs at periods of 8 to 70 s from ambient noise correlation using 12 or more months of continuous data from CNSN, global and regional permanent, and PASSCAL temporary stations. The best observed frequency band is 10 to 30 s with a retrieval rate of 50 to 80% of the station-pairs. We constructed new tomographic maps of China for periods from 8 to 60 s, which correlate with surface geology. Temporal and spatial analyses suggest that the dispersion measurements and tompography are robust. We proposed a bootstrap method, which allowed us to quantify the errors of each of our dispersion curves and the errors of the dispersion maps. For best periods (10–30 s) and most regions, the Rayleigh waves have standard errors of less than 0.1 km/s. We have inverted the dispersion maps for 3D S model (down to about 100 km). The models show remarkable details of the crust and uppermost mantle, including major blocks, rapid changes in Moho, mid/lower crust low velocities in TP, and variations in lithosphere velocities. The resolution is about 4x4 degrees.

REFERENCES

Beaumont, C., R. A. Jamieson, M. H. Nguyen, and B. Lee (2001). Himalayan tectonics explained by extrusion of a low-viscosity crustal channel coupled to focused surface denudation, *Nature* 414: 738–742.

Benson, G., M. Ritzwoller, M. Barmin, A. L. Levshin, F. Lin, M. P. Moschetti, N. M. Shapiro, and Y. Yang (2007). Processing seismic ambient noise data to obtain reliable broad-band surface wave dispersion measurements, *Geophys. J. Int.* 169: (3), 1239–1260.

Campillo, M. (2006). Phase and correlation in random seismic fields and the reconstruction of the Green function, *Pure Appl. Geophys.* 163: 475–502.

Campillo M. and A. Paul (2003). Long-range correlations in the diffuse seismic coda, *Science* 299: 547–549.

Clark, M. K., and L. H. Royden (2000). Topographic ooze: Building the eastern margin of Tibet by lower crustal flow, *Geology* 28: 703–706.

Liang C., X. D. Song, and J. L. Huang (2004). Tomographic Inversion of Pn Travel-Times in China, *J. Geophys. Res.* 109: B11304, doi. 10.1029/2003JB002789.

Lobkis, O. I., and R. L. Weaver (2001). On the emergence of the Greens function in the correlations of a diffuse field, *J. Acoust. Soc. Am.* 110: 3011–3017.

Ritzwoller, M.H. and A. L. Levshin (1998). Eurasian surface wave tomography: Group velocities, *J. Geophys. Res.* 103: 4839–4878 .

Sabra, K.G., P. Gerstoft, P. Roux, W. A. Kuperman, and M. C. Fehler (2005). Surface wave tomography from microseisms in Southern California, *Geophys. Res. Lett.* 32: doi:10.1029/2005GL023155.

Shapiro, N. M., M. Campillo, L. Stehly, and M. H. Ritzwoller (2005). High resolution surface wave tomography from ambient seismic noise, *Science* 307: (5715), 1615–1618.

Shapiro, N. M. and M. H. Ritzwoller (2002). Monte-Carlo inversion for a global shear velocity model of the crust and upper mantle, *Geophys. J. Int.* 151: 88–105.

Song, X. D., X. L. Sun, S. H. Zheng, Z. J. Xu, M. Ritzwoller, and Y. J. Yang (2008). Surface Wave Dispersion Measurements and Tomography from Ambient Seismic Noise in China, in *Proceedings of the 30th Monitoring Research Review: Ground-Based Nuclear Explosion Monitoring Technologies*, LA-UR-08-05261, Vol. 1, pp. 268–278.

Xu, Z., X. D. Song, S. H. Zheng, M. H. Ritzwoller (2008). Bootstrap analysis on surface wave dispersion and tomography derived from ambient noise cross-correlation, *IRIS Workshop*, Skamania Lodge, Stevenson, WA.Zheng, S. H., X. L. Sun, X. D. Song, Y. J. Yang, and M. H. Ritzwoller (2008). Surface wave tomography of China from ambient seismic noise correlation, *Geochem. Geophys. Geosyst.* 9: Q05020, doi:10.1029/2008GC001981.